Periodica Polytechnica
Electrical Engineering
and Computer Science

60(2), pp. 96-106, 2016
DOI: 10.3311/PPee.8873

Predictive Control of Variable Speed Wind Energy Conversion System with Multi Objective Criterions

Said Chikha[1*], Kamel Barra[1]

RESEARCH ARTICLE

Received 04 December 2015; accepted after revision 02 March 2016

Abstract

The paper presents an improved predictive direct rotor current control of a variable speed wind energy conversion system. The conversion chain uses a Doubly Fed Induction Generator DFIG whereas the control method is based on Finite States Space Model Predictive Control FS-MPC of the converter. The proposed control method selects the optimal switching state of the inverter that minimizes the error between orthogonal rotor current components predictions to their computed values. The optimal voltage vector that minimizes a cost function is then applied to the output of the power converter. Once the proposed predictive strategy is validated, multi-level converters well suited for high power application are then used to improve and highlight the obtained results. The proposed predictive control strategy uses only one sample time prediction and it is intuitive since it is very simple for implementation, avoids the cascade structure of several linear controllers and provides best performance.

Keywords

Variable speed wind energy conversion system, DFIG machine, predictive control, finite states-space model, cost function, multi-level converters

[1] Electrical Engineering and Automatic Laboratory LGEA
University of Oum El bouaghi, Algeria

[*] Corresponding author, e-mail: chikhasaid@hotmail.fr

1 Introduction

Nowadays, wind energy conversion has acquired a mature technology and provides a clean and inexhaustible source of energy for maintaining the continuously growing energy needs of humanity.

Compared to other solutions such as fixed-speed induction generators or fully rated converter systems, variable speed Wind Energy Conversion Systems (WECSs) is the most popular used WECS allowing maximum power extraction over a large range of wind speeds. These WECS use generally a Doubly Fed Induction Generator (DFIG) due to its flexibility. The stator winding is directly connected to the grid phases; providing electric power with constant voltage and frequency. The rotor winding is connected to the grid via two back to back power converters (two cascaded converters connected with a direct current DC link). The Rotor Side Converter RSC controls the active and reactive power of the generator while the Grid Side Converter GSC controls the DC link voltage and ensures operation of large power factor. As the rotor speed is fluctuating, the electric power of the rotor is reversible depending on whether the machine operates in either subsynchronous mode or supersynchronous mode. Other advantages of DFIG machines can be cited, such as the adaptability of the power factor, better efficiency and the ability to control the reactive power without capacitive support. Also, they allow a significant reduction of the power converters size and cost since the size of the converters is related to the speed variation range, typically around +/- 30 % of the synchronous speed. Note that the main advantage of the WECS based DFIG machine is the perfect decoupling between active and reactive power control by controlling rotor currents [1-8].

Among the two last decades, several control strategies for WECSs based DFIG have been reported in specialist literature starting from the basic idea that control does significantly improve all aspects of WECS and the most widely used techniques may be classified within the Field Oriented Control (FOC) techniques and the Direct Control techniques (DTC and DPC).

In FOC techniques, the rotor current is decomposed into direct component that controls the torque (the stator active

power) and a quadrature component that commands the rotor flux (stator reactive power) and they are regulated separately with linear PI controllers. In [3-5], the block diagram of the power control of the DFIG incorporates a cascaded structure with four PI regulators, two PIs in the outer loops for stator active and reactive powers and two PIs in the inner rotor currents loops with also an additional PI loop for the speed. As a consequence there exists degradation in the dynamic performance due to delay times of cascaded regulators and reduced robustness against model uncertainties. Simplified structures have been then proposed by eliminating sometimes inner current loops and sometimes the outer power loops but at least the control block contains for three PIs controllers.

Direct Control techniques that originated from Direct Torque Control DTC for induction machines in [2-4] and Direct Self Control DSC in [6] provide direct control of the machine's torque reducing the complexity of the FOC control. These methods have been translated to control DFIG and are different from FOC in that they take into account the discrete nature of power converters and use a switching table to select the appropriate voltage vector to be applied on terminal machine. These techniques provide better transient torque control conditions rather than FOC without requiring current regulators nor coordinate transformations or specific modulations like PWM or SVM for pulse generation since the PI regulators in FOC are eliminated and replaced by hysteresis comparators but they still present some disadvantages compared to FOC such as the lack of direct current control, torque control difficulties at very low speeds and especially variable switching frequency behaviour.

On the other hand, Predictive Direct Power Control P-DPC which is a more sophisticated control method than DTC for direct power control has been recently proposed. The method selects a set of concatenated-voltage vectors, obtaining high-dynamic responses in large-transients. These concatenated-voltage vectors can be built in different forms, combining different design criteria such as conversion efficiency, current ripple or others. There have been some improvements of conventional P-DPC, including the multilevel inverter topologies [20] using two or three vectors during one control period and space vector modulation (SVM) based method [7] etc. Although better performances were obtained, generally the complexity of these methods is also increased.

Recently; Finite-States Model Predictive Control (FS-MPC) appears as a complete and accurate approach to control power converters due to its fast dynamic response, no need for linear controllers in inner loops, no need for modulator (as in PWM or SVM modulation), completely different approach compared to PWM and SVM modulations, extremely simple, good performance and can be implemented with standard commercial microprocessors. The method uses the model of the system to predict for one step ahead prediction the behaviour of the variables for each switching state. For the selection of the appropriate switching state to be applied to the system a quality function must be defined. The cost function is then evaluated for the predicted values on each sampling interval and the optimal switching state that minimizes the quality function is selected to apply during the next sampling interval [17-19].

In this paper, we will extend the application of FS-MPC to WECSs based DFIG since the most papers in this field are mostly related to classic control methods. The superiority of FS-MPC over conventional control will be confirmed by simulation results.

2 WECS Modeling

2.1 Wind turbine characteristic

Several variable-speed WECS configurations are being widely used in literature. The configuration studied in the present paper is a fixed pitch Horizontal Axis Wind Turbines HAWT having a power coefficient (aerodynamic efficiency), C_p depending on the tip speed ratio $\lambda = R\Omega_t / v$ (i.e., the ratio between the blades peripheral speed and the wind speed) having a maximum for λ_{opt} as it is given by Fig. 1. The power characteristics of the wind turbine have a maximum for each wind speed. All these maxima form the so-called Optimal Regimes Characteristics (ORC). The available power on the turbine shaft is given as:

$$P_m = \frac{1}{2} C_p(\lambda) \cdot \rho \cdot \pi \cdot R^2 \cdot v^3 \tag{1}$$

Where ρ is the air density, R is the turbine radius and v is the wind speed (m/s). The turbine torque is the ratio of the output power to the shaft speed.

The power coefficient C_p of the used 2 MW turbine depends on the pitch angle (β) and on the tip-speed ratio λ and can be expressed as [13]:

$$C_p(\lambda,\beta) = (0.35 - 0.00167)(\beta - 2)\sin\left[\frac{\pi(\lambda + 0.1)}{(14.34 - 0.3(\beta + 0.1))}\right] - 0.00184(\lambda - 3)(\beta - 2) \tag{2}$$

Figure 1 depicts the aerodynamic efficiency C_p versus the tip speed ratio λ for different values of the angle β.

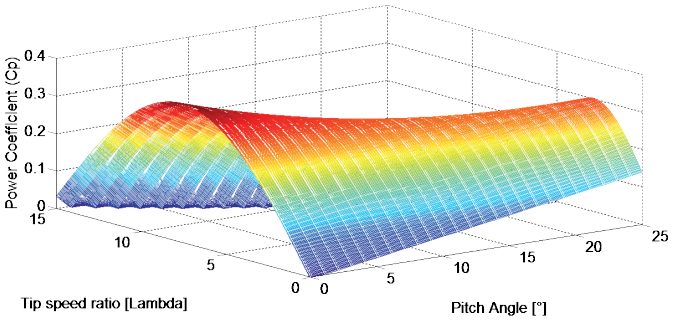

Fig. 1 3 D plot of power coefficient C_p (λ, β)

2.2 DFIG Model

The equations that describe a doubly fed induction generator in a *d-q* reference frame where different parameters of the machine appear in a continue form are identical to those of a squirrel cage induction generator; the only exception is that the rotor winding is not short-circuited. We assume balanced voltages and non-ground connection points. Two orthogonal axes are defined, the d and q axis. The stator and rotor voltages are given by the following equations:

$$\begin{cases} V_{ds} = R_s i_{ds} + \dfrac{d\psi_{ds}}{dt} - \omega_s \psi_{qs} \\ V_{qs} = R_s i_{qs} + \dfrac{d\psi_{qs}}{dt} + \omega_s \psi_{ds} \\ V_{dr} = R_r i_{dr} + \dfrac{d\psi_{dr}}{dt} - \omega_{sl} \psi_{qr} \\ V_{qr} = R_r i_{qr} + \dfrac{d\psi_{qr}}{dt} + \omega_{sl} \psi_{dr} \end{cases} \tag{3}$$

The electromagnetic torque is expressed as:

$$C_{em} = p\left(\psi_{ds} i_{qs} - \psi_{qs} i_{ds}\right) = p\frac{M}{L_r}\left(\psi_{dr} i_{qs} - \psi_{qr} i_{ds}\right) \tag{4}$$

where (V_{ds}, V_{qs}), (i_{ds}, i_{qs}), (ψ_{ds}, ψ_{qs}), (V_{dr}, V_{qr}), (i_{dr}, i_{qr}), (ψ_{dr}, ψ_{qr}) are respectively, the *d-q* stator voltage components, the *d-q* stator current components, the *d-q* stator flux components, the *d-q* rotor voltage components, the *d-q* rotor current components, the *d-q* rotor flux components. R_s and R_r are respectively the stator and rotor resistances. L_s, L_r and M are respectively the stator, rotor and magnetizing inductances. ω_s and ω_{sl} are respectively the synchronous and slip pulsations, p is the pair poles number, s is the slip.

The flux components are given as follows:

$$\begin{cases} \psi_{ds} = L_s i_{ds} + M i_{dr} \\ \psi_{qs} = L_s i_{qs} + M i_{qr} \end{cases} \wedge \begin{cases} \psi_{dr} = L_r i_{dr} + M i_{ds} \\ \psi_{qr} = L_r i_{qr} + M i_{qs} \end{cases} \tag{5}$$

In order to obtain a decoupled control of stator active-reactive powers, the DFIG model requires all quantities to be expressed under stator flux orientation concept and assuming that the stator resistance is small when compared to the stator reactance for medium and high power size machine, the stator flux can be computed as:

$$\begin{cases} \psi_{ds} = \psi_s \\ \psi_{qs} = 0 \end{cases} \rightarrow \psi_s \approx \frac{V_s}{\omega_s} \tag{6}$$

After some manipulations, we can get the stator current components by:

$$\begin{cases} i_{ds} = \dfrac{\psi_s}{L_s} - \dfrac{M}{L_s} i_{dr} \\ i_{qs} = -\dfrac{M}{L_s} i_{qr} \end{cases} \tag{7}$$

Then the torque is simplified into:

$$C_{em} = p\psi_{ds} i_{qs} = -p\frac{M}{L_s}\psi_{ds} i_{qr} \tag{8}$$

The stator active-reactive powers expressions are:

$$\begin{cases} P_s = V_{ds} i_{ds} + V_{qs} i_{qs} = -V_s \dfrac{M}{L_s} i_{qr} \\ Q_s = V_{qs} i_{ds} - V_{ds} i_{qs} = \dfrac{V_s^2}{\omega_s L_s} - \dfrac{V_s M}{L_s} i_{dr} \end{cases} \tag{9}$$

Using the expressions of the rotor active and reactive powers:

$$\begin{cases} P_r = V_{dr} i_{dr} + V_{qr} i_{qr} = s\dfrac{V_s M}{L_s} i_{qr} \\ Q_r = V_{qr} i_{dr} - V_{dr} i_{qr} = s\dfrac{M V_s}{L_s} i_{dr} \end{cases} \tag{10}$$

Then, the total active and reactive powers involved in the grid are expressed by:

$$\begin{cases} P_T = P_s + P_r = (s-1) V_s \dfrac{M}{L_s} i_{qr} \\ Q_T = Q_s + Q_r = \dfrac{V_s^2}{\omega_s L_s} + (s-1) V_s \dfrac{M}{L_s} i_{dr} \end{cases} \tag{11}$$

The dynamics of the rotor current components can be expressed then from relations (3)-(7) by:

$$\begin{cases} V_{dr} = R_r i_{dr} + \sigma L_r \dfrac{di_{dr}}{dt} - s\omega_s \sigma L_r i_{qr} \\ V_{qr} = R_r i_{qr} + \sigma L_r \dfrac{di_{qr}}{dt} + s\omega_s \sigma L_r i_{dr} + s\dfrac{M V_s}{L_s} \end{cases} \tag{12}$$

2.3 Two Level Voltage Source Inverter Model

To describe the inverter output voltages, the concept of complex space vector is applied [16-19]. For a two level voltage source inverter feeding a symmetrical three-phase grid connected system given in Fig. 2, each leg is composed of two by-directional switches (S_{i1}, S_{i2} $i = a, b, c$) where a, b, c the three phases. The switching states S determined by gating signals are given in vectorial form as follows [16]:

$$S = \frac{2}{3}\left(S_a + aS_b + a^2 S_c\right) \tag{13}$$

Where $a = e^{j2\pi/3}$. S_i takes the value of 0 if S_i is off and S_i^* is on, S_i takes the value of 1 if S_i is on and S_i^* is off.

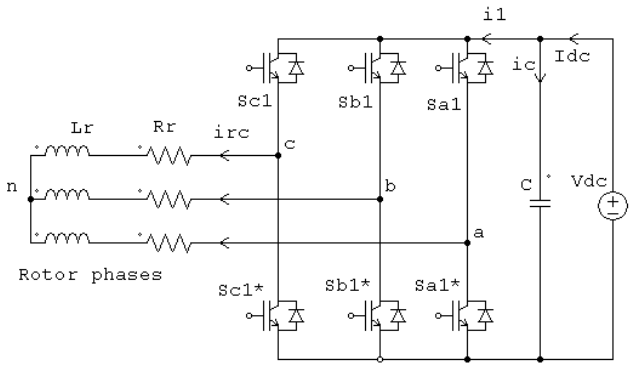

Fig. 2 Tow level voltage source inverter topology

The output voltage space vectors of the inverter are:

$$V = \frac{2}{3}\left(v_{aN} + a v_{bN} + a^2 v_{cN}\right) \tag{14}$$

(v_{aN}, v_{bN}, v_{cN}) are the phase to neutral (N) voltages.

As it is well known, there are eight possible voltage vectors that the inverter can apply to the grid terminals. By using these switching functions the grid space voltage vector can be expressed as [16-19]:

$$V\left(S_a, S_b, S_c\right) = \sqrt{\frac{2}{3}} V_{dc}\left(S_a + S_b e^{j2\pi/3} + S_c e^{j4\pi/3}\right) \tag{15}$$

where V_{dc} is the DC-link voltage.

According to the combination of switching modes, the space vectors V_0 (0,0,0) and V_7 (1,1,1) are the space zero voltage vectors and the others are the space nonzero active voltage vectors as shown in Fig. 3.

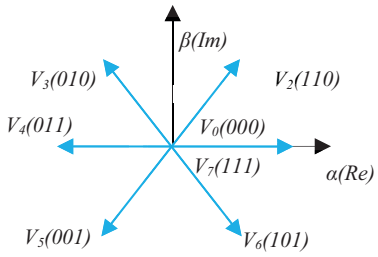

Fig. 3 Representation of different voltage vectors of a two level voltage inverter.

Also, the inverter output voltage is related to DC link voltage by:

$$V = V_{dc} S \tag{16}$$

The inverter output voltage vector is kept constant during the switching period, so the inverter current and, hence, the grid currents can be controlled by choosing the appropriate voltage vector.

3 Control Strategy

Several control algorithms of the WECS have been reported recently through the literature [1-7], whether for a wind system feeding an isolated load, or the network. The configuration of the present work is given by Fig. 5; where the rotor of the DFIG is connected to the grid via a two back to back power converters and a *RL* filter assuming that +/- 30% of the DFIG nominal power is exchanged with the grid whereas the rest of this power is directly generated by the stator to the grid. The Maximum Power Point Tracker MPPT controller is used to track closely the maximum power point of the wind turbine (turbine rotor works closely on the Optimal Regime Characteristic ORC).

3.1 MPPT control

In order to obtain the maximum captured energy from the wind, the designed controller should guarantee that the turbine is kept on the MPPT curve as the wind velocity changes. The based control is to adjust the electromagnetic torque on the shaft of the DFIG in order to fix the rotational speed to a reference value. To achieve this, a control of the rotation speed of the DFIG has to be performed, the electromagnetic reference torque C^*_{em} is obtained at the output of the speed PI controller as it is shown by Fig. 4. This controller allows the tracking of the DFIG rotational speed and mitigates the effect of mechanical torque C_{em} considered as a perturbation [9-11].

For a given operating point (fixed speed wind), it is desired that the mechanical power is maximum, which corresponds to the maximum value of the coefficient $C_{p\text{-max}}$. This is obtained if the relative velocity λ reaches its optimal value λ_{opt} (for a pitch angle β constant and equal to 2° in our case study).

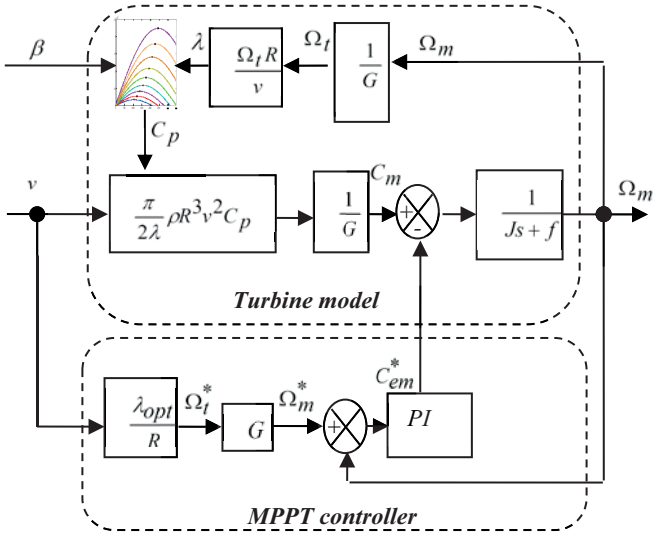

Fig. 4 MPPT controller

The reference rotational speed of the turbine Ω_t^* is then obtained from the Eq. (2) and it is defined by:

$$\Omega_t^* = \frac{\lambda_{opt} v}{R} \tag{17}$$

We deduce then the reference speed of the DFIG taking into account the gain of the multiplier G (gear box multiplier) by:

$$\Omega_m^* = G \cdot \Omega_t^* \tag{18}$$

3.2 Control of DFIG

Generally, the field oriented control (FOC) concept of the DFIG is based on stator active-reactive power control, however this solution is suitable only when the machine operates in normal regime, but when the grid is affected by disturbances and faults which is not considered in this study, the measure of stator powers is not appropriate, so the rotor currents are chosen to be directly controlled [10-14].

The rotor currents references can be expressed by:

$$i_{qr}^* = -\frac{L_s}{pM\psi_s} C_{em}^* \tag{19}$$

$$i_{dr}^* = \frac{\psi_s}{M} - \frac{L_s}{MV_s} Q_s^* \tag{20}$$

The reference for the stator active power P_s^* is then given as:

$$P_s^* = \frac{\omega_s}{p} \cdot C_{em}^* \tag{21}$$

The stator reactive power Q_s^* is set to 0. The global control structure of the studied WECS using two back to back voltage source converter VSI is given by Fig. 5.

4 Predictive Control

4.1 Predictive model

The rotor current components can be expressed from relations (12) by:

$$\begin{cases} \dfrac{di_{dr}}{dt} = \dfrac{1}{\sigma L_r}\left(V_{dr} - r_r i_{dr} + s\omega_s \sigma L_r i_{qr}\right) \\ \dfrac{di_{qr}}{dt} = \dfrac{1}{\sigma L_r}\left(V_{qr} - r_r i_{qr} - s\omega_s \sigma L_r i_{dr} - s\dfrac{MV_s}{L_s}\right) \end{cases} \tag{22}$$

Where V_{dr}, V_{qr} are the output voltage space vectors generated by the inverter.

Prediction of rotor current components can be made for one step ahead prediction as:

$$\begin{cases} i_{dr}(k+1) = \dfrac{T}{\sigma L_r}\left(V_{dr}(k) - r_r i_{dr(k)} + s\omega_s \sigma L_r i_{qr}(k)\right) \\ \qquad\qquad + i_{dr}(k) \\ i_{qr}(k+1) = \dfrac{T}{\sigma L_r}\left(V_{qr}(k) - \mathrm{r_r i_{qr}}(k) - s\omega_s \sigma L_r i_{dr}(k) - s\dfrac{MV_s}{L_s}\right) \\ \qquad\qquad + i_{\mathrm{qr}}(k) \end{cases} \tag{23}$$

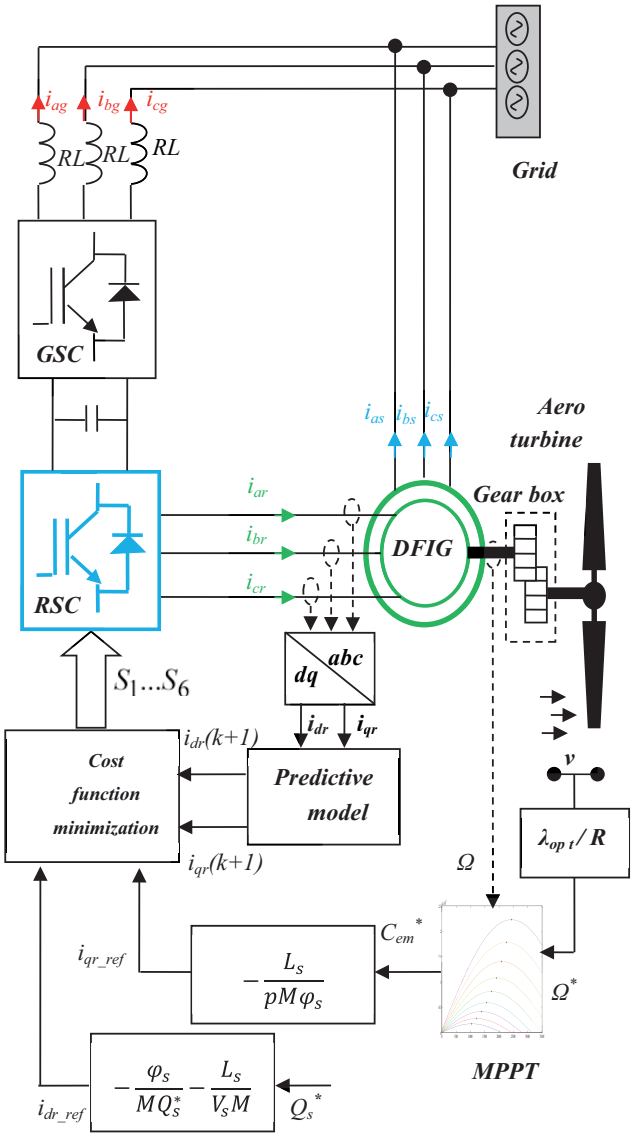

Fig. 5 Predictive control for WECS.

4.2 Minimization of cost function

The control objective is to get high performance in term of rapid and precise dynamic current control response by using a cost function that minimizes the error between reference currents to their computed values. The predictions on rotor currents are used to evaluate the impact of every voltage vector on the WECS. The cost function is formulated as:

$$C_{[7]} = \left|i_{dr}^*(k+1) - i_{dr}(k+1)\right| + \left|i_{qr}^*(k+1) - i_{qr}(k+1)\right| \tag{24}$$

The flow chart of the predictive control is given by Fig. 6, where for each rotor voltage vector the cost function C is evaluated and the optimal voltage vector is then applied during the next sampling period [17-19].

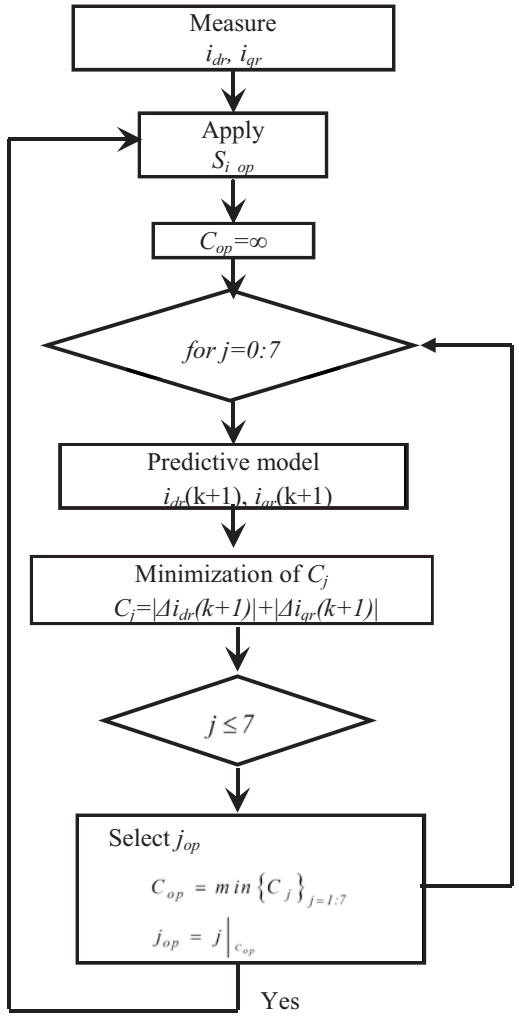

Fig. 6 Flow chart of the predictive algorithm [17-19].

5 Simulation results

The proposed predictive control of the studied WECS given by Fig. 5 is tested in Matlab environment with a sampling time of 100µs, considering a DFIG of 2MW for high power generation system whose parameters are given in the appendix. The results are presented in order to show the performance, the speed time response, and the accurate of the tracking reference. The wind speed profile is given by Fig. 7.

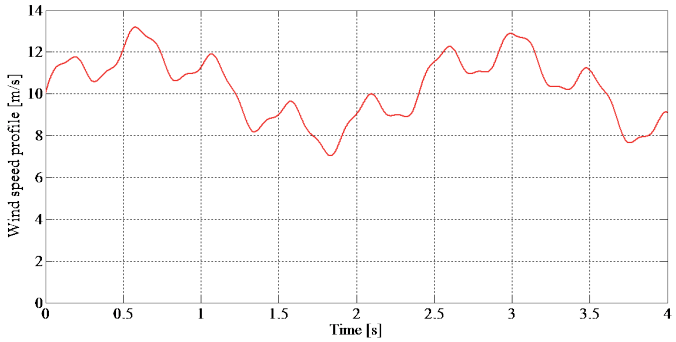

Fig. 7 Wind speed profile.

In Fig. 8, the rotor line currents against speed generator variation are depicted for both subsynchronous and supersynchronous regimes.

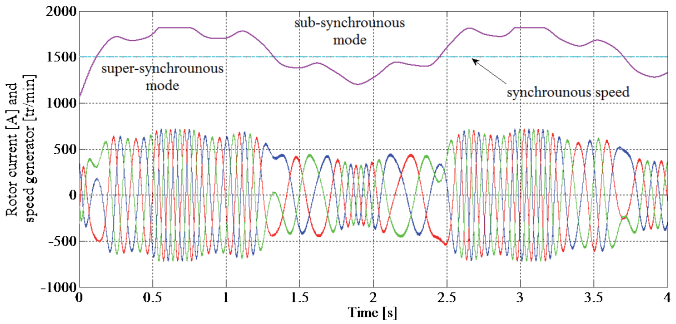

Fig. 8 Rotor currents versus speed generator.

In Fig. 9, We can see the good performance obtained with the proposed control in term of good reference tracking performance. The generated stator active and reactive powers are illustrated by Fig. 9 for a stator reactive power reference settled to 0 VAR. The tracking performance shows high dynamic performance for both stator powers since the powers are perfectly decoupled and track their references accurately and precisely. As a consequence, the stator current in Fig. 10 appears highly sinusoidal and is achieved in opposite phase with the grid-stator voltage because the machine operates in subsynchronous mode.

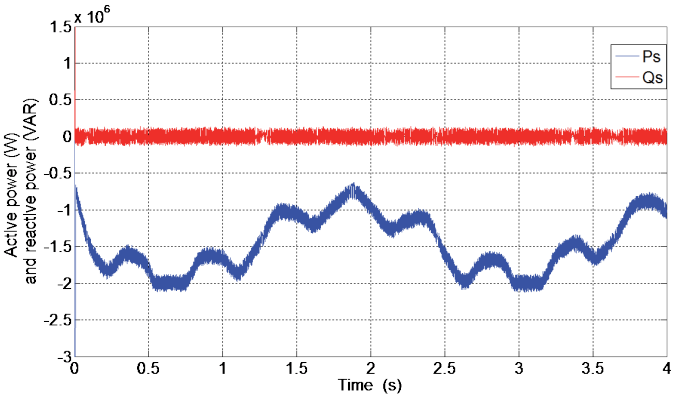

Fig. 9 Stator active and reactive power.

6 Predictive Control with switching frequency reduction

Reduction of switching frequency for high power wind energy application is very important to improve the efficiency by reducing the power losses due to commutations in the inverter. One of the most benefits of finite states predictive control is its flexibility since we can add nonlinear constraints which are usually difficult to consider in linear controllers by adding more terms in the cost function to be minimised [17-19]. Here a third term that takes into account the reduction of the switching frequency without degradation of the reference tracking performance is added to the objective function of (25) by:

$$C_{[7]} = \left|i_{dr}^{*}(k+1) - i_{dr}(k+1)\right| + \left|i_{qr}^{*}(k+1) - i_{qr}(k+1)\right| + \lambda \sum_{\substack{k=a,b,c \\ j=1:8}} \left(V_{kr}(j) - V_{kr_{opt}}(j)\right) \tag{25}$$

where:

$$\begin{cases} V_{ar}(j) = S(1,j)\cdot V_{dc} \\ V_{br}(j) = S(2,j)\cdot V_{dc} \\ V_{cr}(j) = S(3,j)\cdot V_{dc} \end{cases} \tag{26}$$

The last term in (25) is the number of commutations required to switch from the optimal present switching state to the switching state under evaluation. The parameter λ is a weighting factor chosen according to the desired performance.

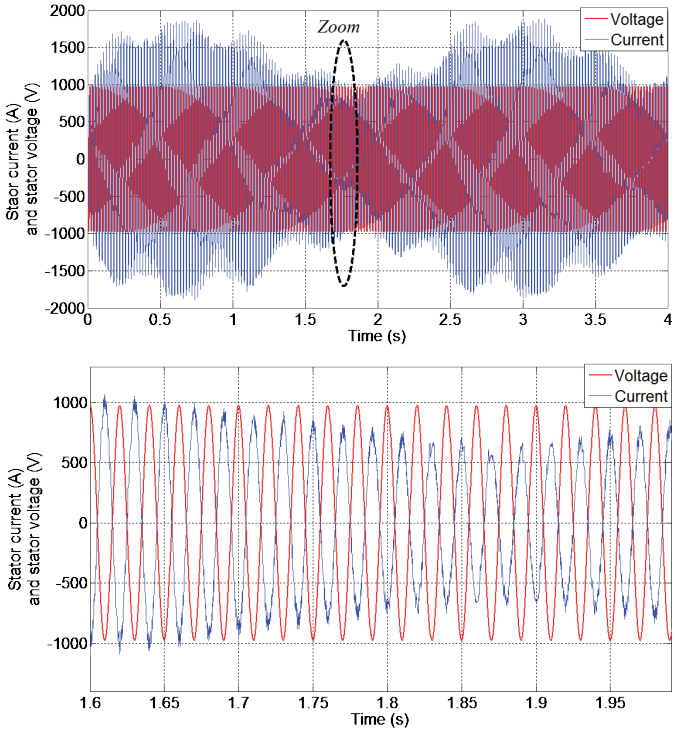

Fig. 10 Stator current vs. stator voltage (The bottom curve represents the zoom of the curve at the top)

6.1 Selection of weighting factor

The choose of the weighting factor value can be considered as the hard task of the method since several tests have been used to select the better variation interval for λ.

By using the cost function (25), the behaviour of the rotor currents, the number of commutation and switching frequency for different values of λ for this special example, where the wind speed is set constant at 11m/s, are given by Figs. 11-13.

As can be seen from these figures that switching frequency can be reduced by increasing the weighting factor but on the other hand high values of λ can deteriorate the reference tracking performance of rotor currents as it can be seen by Fig. 11, so a compromise between reduction of the switching frequency to an acceptable level and good tracking performance should be made.

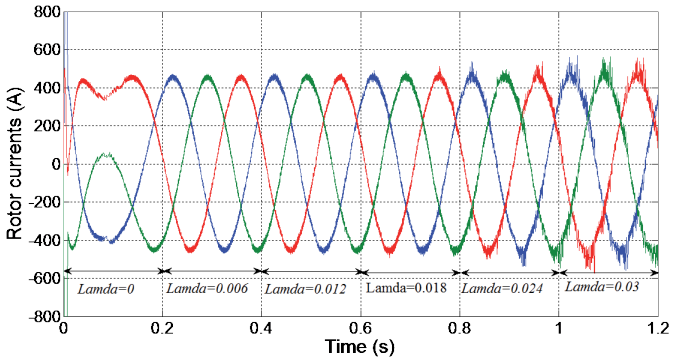

Fig. 11 Rotor currents for different values of λ (V_{wind} = 11m/s)

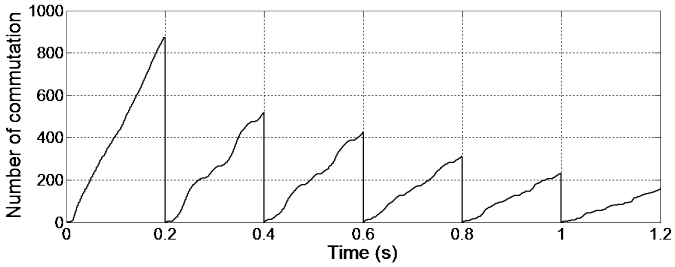

Fig. 12 Reduction of the switching number for different values of λ of Fig. 11.

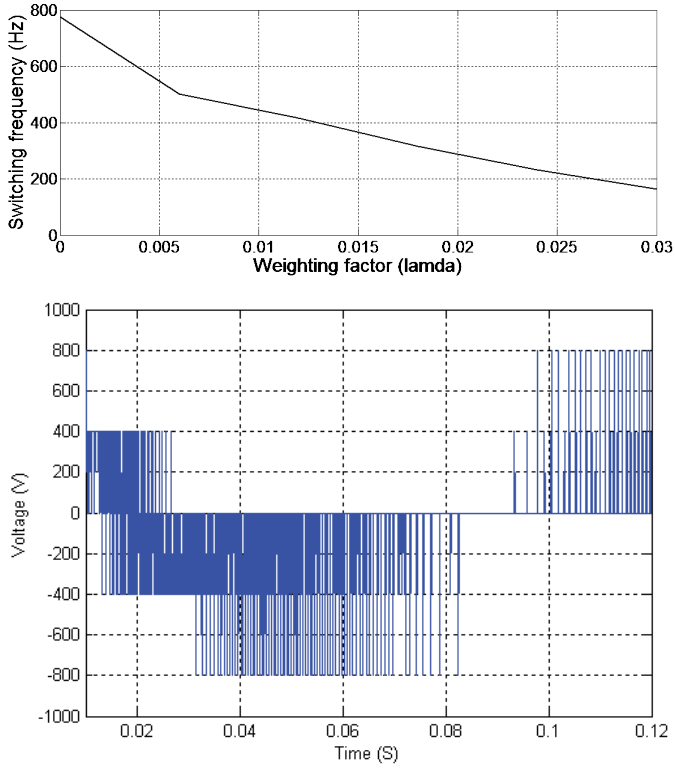

Fig. 13 Reduction of switching frequency by increasing λ

7 Interest of multilevel converters for wind energy conversion

Two level voltage source inverters (2L-VSI) are widely used in wind energy conversion for low voltage low power applications [20-21]. In medium voltage high power systems multilevel converters are used due to several advantages over the traditional two-level converters, such as, operation with voltages over the switching devices rating, reduced common-mode

voltages, smaller voltage changes (*dv/dt*) and low harmonic distortion THD. Also, it was proofed in such system that the transited active power via a multilevel inverter having (n + 1) voltage levels with unity power factor is (n) times that can be transited with (n) inverters having two voltage levels.

In order to improve the obtained results, two topologies of multilevel converters suitable for this high power application are used, namely a three level Neutral Point Clamped converter (3L-NPC) and a four level NPC converter (4L-NPC) converter. The power circuits are shown in Fig. 14 and Fig. 15.

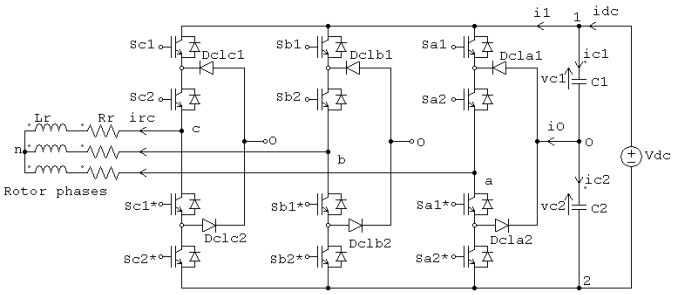

Fig. 14 Three level Neutral Point Clamped inverter topology (3L-NPC)

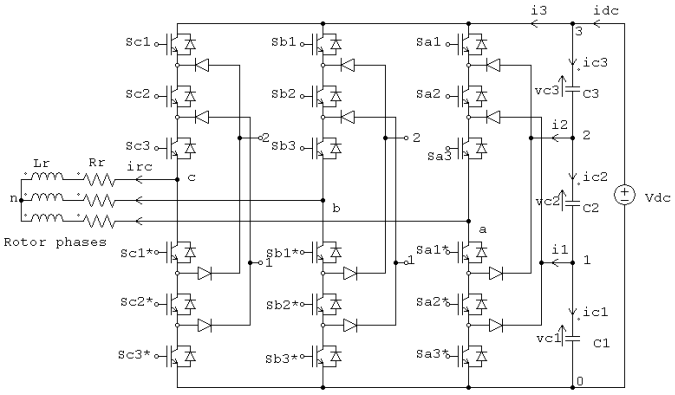

Fig. 15 Four level Neutral Point Clamped inverter topology (4L-NPC)

It is well known that a multilevel converter having (n + 1) voltage levels is supplied by n input capacitors and when it is connected to a three phase load the converter applies to the load ($3n^2 + 3n + 1$) different voltage vectors generated from n^3 switching states as it is presented in Fig. 16. In 3L-NPC topology, there are 27 switching states; only 19 different voltage vectors are applied to terminal rotor machine whereas in 4L-NPC structure there are 64 switching states, only 37 different voltage vectors are applied by the RSC converter as given by Fig. 17.

The main drawback of these multilevel converters is the unbalance voltages of the DC link capacitors in the input side converter. To improve the results of the wind energy conversion system in term of high efficiency, low electromagnetic ripples, low power oscillations and low harmonics on current waves without unbalance of the DC-link voltage capacitors, the cost function is now formulated for both topologies as:

For the 3L-NPC:

$$C_{[27]} = \left|i_{dr}^{*}(k+1) - i_{dr}(k+1)\right| + \left|i_{qr}^{*}(k+1) - i_{qr}(k+1)\right| + \alpha\left|V_{c1}(k+1) - V_{c2}(k+1)\right| \tag{27}$$

for the 4L-NPC:

$$C_{[64]} = \left|i_{dr}^{*}(k+1) - i_{dr}(k+1)\right| + \left|i_{qr}^{*}(k+1) - i_{qr}(k+1)\right| + \beta\left[\left|V_{c1}(k+1) - V_{c2}(k+1)\right| + \left|V_{c2}(k+1) - V_{c3}(k+1)\right| + \left|V_{c3}(k+1) - V_{c1}(k+1)\right|\right] \tag{28}$$

The third term in (27) and (28) evaluates the error of the input capacitor voltages. The parameters α, β are weighting factors that allows to adjust the importance of different terms in the cost function.

By setting weighting factors to $\alpha = 0$ and $\beta = 0$, Figs. 18 and 19 show the enhancement of stator active and reactive powers of multilevel structures in term of reduced oscillations and ripples that improves the efficiency of the wind energy conversion chain.

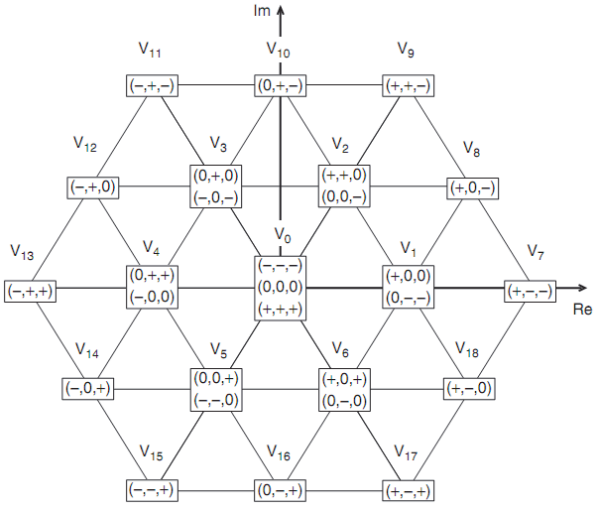

Fig. 16 Possible voltage vectors for a 3L-NPC topology (19 voltage vectors)

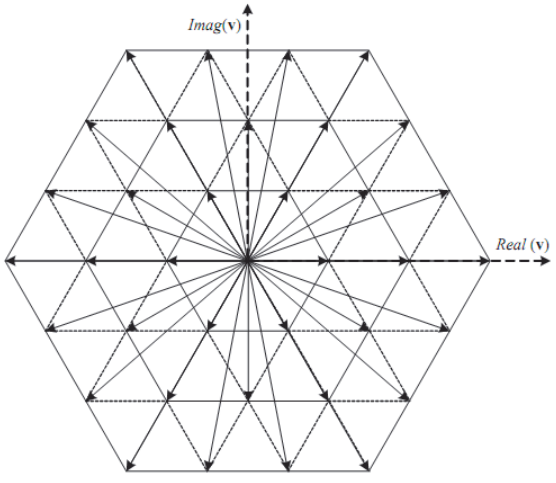

Fig. 17 Possible voltage vectors for a 4L-NPC topology (37 voltage vectors)

In order to control the input DC-Link voltage of the input capacitors, the weighted factors are now settled in the range [0-2s] to $\alpha = 0,\ \beta = 0$ and to $\alpha = 0.1,\ \beta = 0.12$ in the range [2-4s]. Note that the the capacitor voltage reference is defined as $V_{dc}^{*} = Vdc/2$ for the 3L-NPC structure and $V_{dc}^{*} = Vdc/3$ for the 4L-NPC topology. On the results shown in Fig. 20 and Fig. 21, one can see that the capacitor voltages are out of balance when $\alpha = 0,\ \beta = 0$ and can deteriorate the current waveforms by adding some harmonics in their THD but when the weighting factors are settled to $\alpha = 0.1,\ \beta = 0.12$, the capacitor voltages are controlled and the DC-Link voltage is correctly at its true value and consequently reduces some harmonics in the current waveforms.

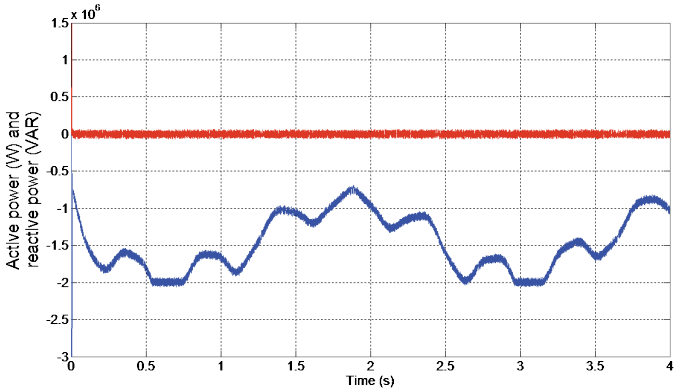

Fig. 18 Stator powers for 3L-NPC topology

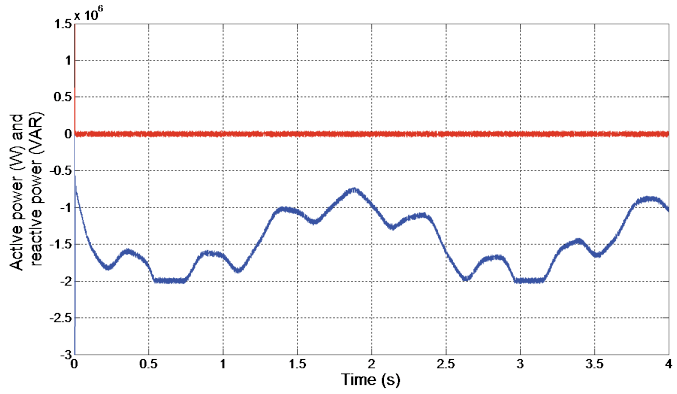

Fig. 19 Stator powers for 4L-NPC topology

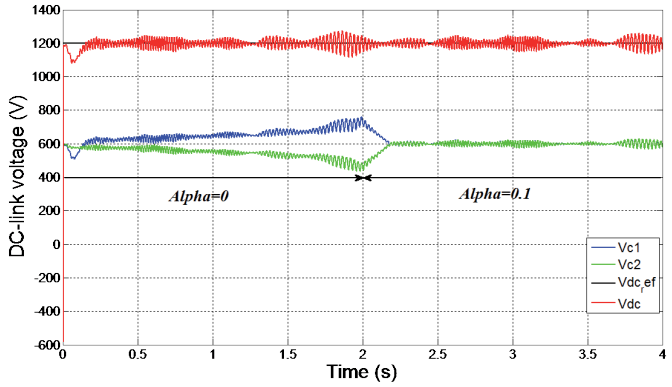

Fig. 20 DC-link voltage for 3L-NPC topology

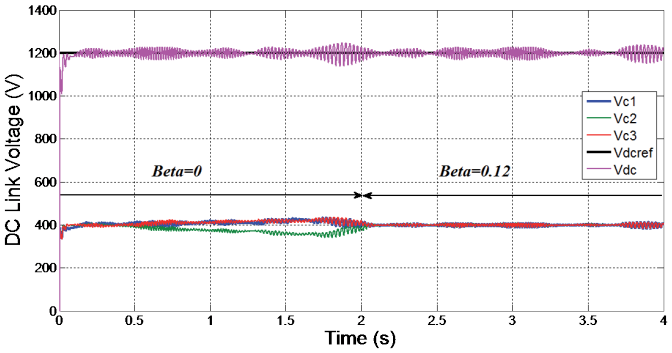

Fig. 21 DC-link voltage for 4L-NPC topology.

Also, Figs. 22-24 show the improvement of stator currents THD where it clear to see that as the number of voltage levels increases the current THD decreases justifying the use of multilevel converters in high power applications, (THD of 3.57 % for the 2L-NPC, 2.70 % for the 3L-NPC and 1.29 % for the 4L-NPC topology).

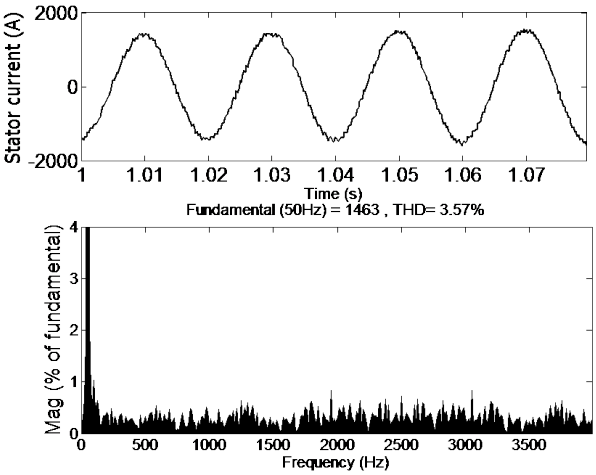

Fig. 22 Stator current THD (2L-VSI)

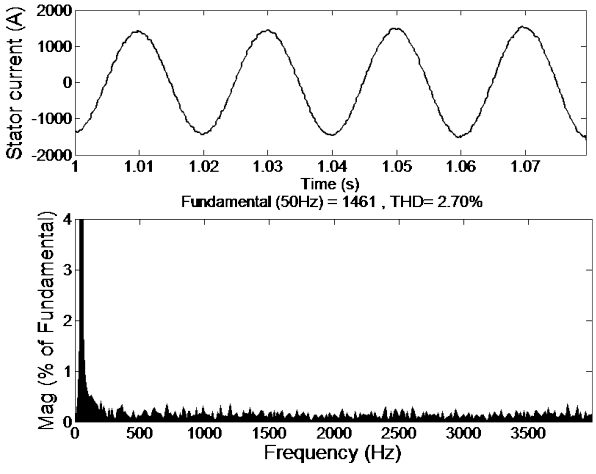

Fig. 23 Stator current THD (3L-NPC-VSI).

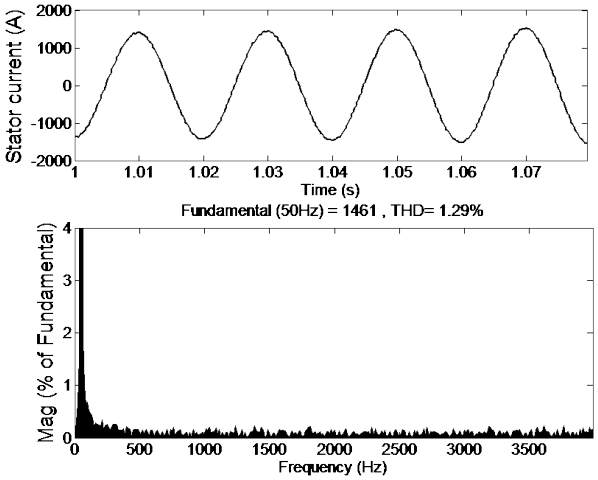

Fig. 24 Stator current THD (4L-NPC-VSI)

8 Conclusion

A predictive rotor current control strategy with multi objective criterions is proposed and applied to control a wind energy conversion chain based on a doubly fed induction generator using different topologies of power electronic converters. The most advantage of the proposed control method is its simplicity in implementation, since the method avoids the use of linear or nonlinear controllers except for the external wind speed loop and there is no need for any type of modulator, such as in PWM modulation, which can reduce the overall cost of the drive system. The control scheme is very simple and uses discrete model of the converter to predict the behavior of rotor currents and to obtain the best suited converter switching state. The method is very flexible since cost functions are used to control many objectives simultaneously by adding more terms that take into account for reduction of the switching commutation frequency and balance voltage of the input capacitors. Simulation results show accurate tracking performance of rotor currents with a significant reduction of oscillation of stator powers that improves the efficiency of the conversion chain.

The multilevel converters have many benefits in high power systems since they provide low ripple on powers and low harmonic distortion on stator currents where it is confirmed that as the number of voltage levels increases the current THD decreases. To cope with the unbalance voltage capacitors, a third term that minimises the voltage capacitor errors is added in the cost function. The results show that it is possible to overcome to this drawback due to the flexibility of the method.

Appendix

Variables	Description	Simulation value
Source		
V_s	RMS supply stator voltage phase (V)	690
f_s	Supply Frequency (Hz)	50
DFIG		
P_n	Nominal power (MW)	2
R_r	Rotor Resistance ($m\Omega$)	55.44
R_s	Stator Resistance ($m\Omega$)	4.45
M	Mutual Inductance (mH)	4.41
L_s	Stator Inductance (μH)	134
L_r	Rotor Inductance (mH)	1.6
P	Number of pair of the pole	2
Turbine		
R	Rotor blades	3
N_{tn}	Nominal rotational speed (tr/min)	19.5
G	Multiplication of gear box	80

References

[1] Taib, N., Metidji, B., Rekioua, T. "Performance and efficiency control enhancement of wind power generation system based on DFIG using three level sparse matrix converter." *Electric Power And Energy Systems Journal*. 53, pp. 287-296. 2013. DOI: 10.1016/j.ijepes.2013.05.019

[2] Foo, G., Rahman, M. F. "Direct torque and flux control of an IPM synchronous motor drive using a back stepping approach." *IET Electric Power Applications*. 3(5), pp. 413. 2009. DOI: 10.1049/iet-epa.2008.0182

[3] Bevilaqua, M. A., Nied, A., de Oliveira, J. "Labview FPGA FOC implementation for synchronous Permanent Magnet Motor Speed Control." In: 2014 11th IEEE/IAS International Conference on Industry Applications (INDUSCON), Juiz de Fora, Brasil, December 7-10, 2014. pp. 1-8. DOI: 10.1109/INDUSCON.2014.7059427

[4] Kowalski, C. T., Lis, J., Orlowska-Kowalska, T. "FPGA implementation of DTC control method for induction motor drive." In: EUROCON, 2007. The International Conference on "Computer as a Tool". Warsaw, Poland, September 9-12, 2007. pp. 1916-1921. DOI: 10.1109/EURCON.2007.4400657

[5] Akhmatov, V. "Modelling and Ride-through Capabilities of Variable Speed Wind Turbines With Permanent Magnet Generators." *Wind Energy*. 9(4), pp. 313-326. 2006. DOI: 10.1002/we.174

[6] Denpenbrock, M. "Direct Self Control DSC of inverter fed induction machine." Power Electronics Specialists Conference, 1987 IEEE, Blacksburg, VA, USA, June 21-26, 1987. pp. 632-641. DOI: 10.1109/PESC.1987.7077236

[7] Verij, K. M., Sadeghi, Y. A., Kojabadi, H. K. "Direct power control of DFIG based on discrete space vector modulation." *Renewable Energy*. 35(5), pp. 1033-1042. 2010. DOI: 10.1016/j.renene.2009.09.008

[8] Zaragoza, J., Pou, J., Arias, A., Spiteri, C., Robles, E., Ceballos, S. "Study and experimental verification of control tuning strategies in a variable speed wind energy conversion system." *Renewable Energy.* 36(5), pp. 1421-1430. 2011. DOI: 10.1016/j.renene.2010.11.002

[9] Akel, F., Ghennam, T., Berkouk, E. M., Laour, M. "An improved sensorless decoupled power control scheme of grid connected variable speed wind turbine generator." *Energy Conversion and Management*. 78, pp. 584-594. 2014. DOI: 10.1016/j.enconman.2013.11.015

[10] Merahi, F., Berkouk, E. M., Mekhilef, S. "New management structure of active and reactive power of a large wind farm based on multilevel converter." *Renewable Energy.* 68, pp. 814-828. 2014. DOI: 10.1016/j.renene.2014.03.007

[11] Mesbahi, T., Ghannem, T., Berkouk, E. M. "A Doubly Fed Induction Generator for wind stand-alone power applications (Simulation and experimental validation)." In: Electrical Machines (ICEM), 2012 XXth International Conference, Marseille, Fance, September 2-5, 2012. pp. 2028-2033. DOI: 10.1109/ICElMach.2012.6350161

[12] Bouharchouche, A., Berkouk, E. M., Ghennam, T., Tabbache, B. "Modeling and control of a Doubly fed induction generator with battery-super capacitor hybrid energy storage for wind power application." In: Power Engineering, Energy and Electrical Drives, Fourth International Conference, Istanbul, Turkey, May 13-17, 2013. pp. 1392-1397. DOI: 10.1109/PowerEng.2013.6635818

[13] Selma, E. A. "Modelling and control structures for variable speed wind turbine." In: Multimedia Computing and Systems (ICMCS), International Conference, Ouarzazate, Morocco, April 7-9, 2011. pp. 1-5. DOI: 10.1109/ICMCS.2011.5945670

[14] Munteanu, I., Bratcu, A. I., Cutululis, N.-A., Ceanga, E. "*Optimal control of wind energy systems, towards a global approach.*" Springer-Verlag London, 2008. DOI: 10.1007/978-1-84800-080-3

[15] Munteanu, I., Bacha, S., Bratcu, A. I., Guiraud, J., Roye, D. "Energy-reliability optimization of wind energy conversion systems by sliding mode control." *IEEE Transactions on Energy Conversion.* 23(3), pp. 975-985. 2008. DOI: 10.1109/TEC.2008.917102

[16] Barra, K., Rahem, D. "Predictive direct power control for photovoltaic grid connected system: an approach based on multilevel converters." *Energy Conversion and Management*. 78, pp. 825-833. 2014. DOI: 10.1016/j.enconman.2013.06.064

[17] Vargas, R., Cortes, P., Ammann, U., Rodriguez, J., Pont, P. "Predictive control of three-phase neutral point clambed inverter." *IEEE Transactions on Industrial Electronics.* 54(5), pp. 2697-2705. 2007. DOI: 10.1109/TIE.2007.899854

[18] Rodriguez, J., Pontt, J., Silva, C., Salgado, M., Rees, S., Ammann, U., Lezana, P., Huerta, R., Cortes, P. "Predictive control of three phase inverter." *Electronics Letters.* 40(9), pp. 561-563. 2004. DOI: 10.1049/el:20040367

[19] Cortes, P., Rodriguez, J., Quevedo, D., Silva, C. "Predictive current control strategy with imposed load current spectrum." *IEEE Transactions on Power Electronics.* 23(2), pp. 612-618. 2008. DOI: 10.1109/TPEL.2007.915605

[20] Perantzakis, G. S., Xepapas, F. H., Manias, S. N. "Efficient predictive current control technique for multilevel voltage source inverters." In: Power Electronics and Applications, 2005 European Conference, Dresden, Germany, September 11-14, 2005. DOI: 10.1109/EPE.2005.219543

[21] Busquets-Monge, S., Bordonau, J., Rocabert, J. "Extension of the nearest-three virtual-space-vector PWM to the four-level diode-clamped dc-ac converter." Power Electronics Specialists Conference, 2007. PESC 2007. IEEE, Orlando, FL, USA, June 17-21, 2007. pp. 1892-1898. DOI: 10.1109/PESC.2007.4342291